Effect of the O6 Substituent on Misincorporation Kinetics Catalyzed by DNA Polymerases at O^6-Methylguanine and O^6-Benzylguanine†

Adrienne M. Woodside‡ and F. Peter Guengerich*

Department of Biochemistry and Center in Molecular Toxicology, Vanderbilt University School of Medicine, Nashville, Tennessee 37232-0146

Received July 17, 2001; Revised Manuscript Received September 26, 2001

ABSTRACT: Misincorporation at a DNA−carcinogen adduct may contribute to formation of mutations if a polymerase proceeds past the lesion, compromising fidelity, as in the G:C to A:T mutations caused by O^6-alkylguanine. Replication of primer/templates containing guanine (G), O^6-methylguanine (O^6-MeG), or O^6-benzylguanine (O^6-BzG) was assessed using T7 DNA polymerase exo$^-$ (T7$^-$) and HIV-1 reverse transcriptase (RT). The steady-state parameters indicated that T7$^-$ and RT preferentially incorporated dTTP opposite O^6-MeG and O^6-BzG. The incorporation efficiencies (k_{cat}/K_m) were less for O^6-BzG than O^6-MeG for both dCTP and dTTP insertion. Pre-steady-state analysis indicated that the product formed during the burst phase, i.e., the burst amplitude, differed significantly between the unmodified 24-mer/36-G-mer and the O^6-alkylG-containing substrates. Extension of the O^6-BzG-containing duplexes was much more difficult for both polymerases as compared to O^6-MeG, except when RT easily extended the O^6-BzG:T base pair. The K_d^{dNTP} for binding of dCTP or dTTP to a RT•DNA complex containing O^6-MeG was 8-fold greater than for dNTP binding to a complex containing unmodified DNA. The K_d^{dNTP} for a RT•DNA complex containing O^6-BzG was 50-fold greater. In conclusion, the bulkier O^6-BzG is a greater block to polymerization by T7$^-$ and RT than is O^6-MeG, but some polymerization does occur with an O^6-BzG substrate. Pre-steady-state analysis indicates that neither dCTP nor dTTP insertion is strongly preferred during polymerization of O^6-BzG-containing DNA, unlike the case of O^6-MeG. These results and others regarding polymerase stalling opposite O^6-MeG and O^6-BzG are discussed in the following paper in this issue [Woodside, A. M., and Guengerich, F. P. (2002) *Biochemistry 41*, 1039−1050].

Maintenance of genomic integrity is essential for cell survival, and the stability of DNA can be compromised with exposure to exogenous and endogenous chemicals of varying structure (*1*, *2*). Once inside the cell, a chemical can be subsequently activated to a potent electrophile (*2*, *3*), which can then react with DNA to yield a covalent modification of the nucleotide base, i.e., a DNA adduct (*4*). Because many DNA lesions have potent miscoding abilities, mutations can result if the lesion escapes repair and the polymerase inserts an incorrect nucleotide opposite the adduct during replication (*5*−*8*). Thus, polymerase fidelity in the presence of a DNA adduct is of paramount importance.

Nitrosamines and nitrosamides are environmental carcinogens (*4*, *9*) that may also be formed in vivo (*10*). These chemicals have been implicated in the alkylation of nucleophilic sites in DNA (*4*). Although N^7-alkylG[1] is the most prevalent lesion formed, O^6-alkylated derivatives of G are believed to be the most carcinogenic lesions that result following nitrosamine and nitrosamide reaction with DNA (*11*). The miscoding potential of O^6-MeG is due to polymerase insertion of T opposite O^6-MeG, resulting in GC to AT transition mutations (*8*).

NMR studies of DNA duplexes containing O^6-MeG:C (*12*) and O^6-MeG:T pairs (*13*) indicate that the wobble base pair O^6-MeG:C is more stable than the pseudo-Watson−Crick base pair O^6-MeG:T in duplex DNA. In addition, the O^6-MeG:C base pair has more hydrogen bonds than O^6-MeG:T (*12*, *13*), but T is preferentially incorporated across from O^6-MeG, dispelling the notion that only hydrogen bonding of base pairs dictates which base is inserted. Rather, incorporation of T opposite O^6-MeG is preferred due to the ease of phosphodiester bond formation for an O^6-MeG:T base pair, which has geometric similarity to a Watson−Crick base pair (*14*).

† This work was supported in part by United States Public Health Service (USPHS) Grants R35 CA44353, R01 ES10546, and P30 ES00267.

‡ Formerly Adrienne N. Mican. Supported in part by USPHS T32 ES07028.

* To whom correspondence should be addressed at the Department of Biochemistry and Center in Molecular Toxicology, Vanderbilt University School of Medicine, 638 Robinson Research Building, 23rd and Pierce Avenues, Nashville, TN 37232-0146. Telephone: (615) 322-2261. Fax: (615) 322-3141. E-mail: guengerich@toxicology.mc.vanderbilt.edu.

[1] Abbreviations: G, guanine; C, cytosine; T, thymine; O^6-alkylG, O^6-alkylguanine; O^6-MeG, O^6-methylguanine; O^6-BzG, O^6-benzylguanine; N^7-alkylG, N^7-alkylguanine; Bz, benzyl; dG, 2′-deoxyguanosine; 8-oxoG, 8-oxo-7,8-dihydroguanine; AF-G, *N*-(deoxyguanosin-8-yl)-2-aminofluorene; AAF-G, *N*-(deoxyguanosin-8-yl)-2-acetylaminofluorene; cisplatin, *cis*-diamminedichloroplatinum(II); T7$^-$, T7 DNA polymerase exo$^-$; RT, human immunodeficiency virus-1 reverse transcriptase; KF, *Escherichia coli* polymerase I (Klenow fragment); E, enzyme (used when describing complexes that include the polymerase); EDTA, (ethylenedinitrilo)tetraacetic acid; Tris, tris(hydroxymethyl)aminomethane; DTT, DL-dithiothreitol; BSA, bovine serum albumin; 1× TBE, 90 mM Tris-borate buffer (pH 8.5) containing 2.0 mM EDTA; TLC, thin-layer chromatography; DMT, dimethoxytrityl; PheAc, phenoxyacetyl; HPLC, high-performance liquid chromatography; CGE, capillary gel electrophoresis; MALDI/TOF MS, matrix-assisted laser desorption ionization/time-of-flight mass spectrometry.

10.1021/bi011495n CCC: $22.00
Published on Web 12/27/2001

The mutagenicity of O^6-MeG has been characterized in a number of studies using site-specific mutagenesis and steady-state incorporation experiments. Sequence contexts can affect the polymerase preference for incorporation of T over C (*8*). Also, some polymerases are blocked at the site of O^6-MeG, which can affect misincorporation efficiency (*15*). Genetic and biochemical evidence indicates that both yeast polymerase δ and polymerase η bypass O^6-MeG in vivo, but polymerase η is more accurate and efficient than polymerase δ (*16*).

Pre-steady-state kinetic analysis is utilized to determine the rates of individual steps in the polymerization cycle (*17*−*19*) for evaluation of their roles during incorporation. Pre-steady-state experiments by Tan et al. (*20*) with polymerase I (KF, exonuclease$^+$), a repair polymerase in *Escherichia coli*, indicate a 5-fold difference in phosphodiester bond formation for the incorporation of T as compared to C. This difference in bond formation may play a role in the mutagenicity of O^6-MeG. Understanding polymerase enzymology in the presence of a DNA lesion can provide insight into how adducts perturb polymerization and allow the incorporation of the wrong base.

In this paper and the following one in this issue (*21*), misincorporation opposite O^6-MeG and O^6-BzG by the replicative polymerases T7$^-$ and RT was investigated using steady-state and pre-steady-state kinetic analysis. O^6-MeG and O^6-BzG were chosen as substrates to provide general insight regarding how bulk at the O6 position affects the interaction of the DNA with the polymerase. Previous studies have confirmed the mutagenicity of O^6-MeG, but the miscoding potential of the bulkier O^6-BzG is not understood as well (*22*). Model replicative polymerases and pre-steady-state kinetics can be used to further our current understanding of how O^6-MeG and O^6-BzG affect replication. Results indicated that both polymerases preferentially extended the O^6-MeG:T base pair, but RT extended the O^6-BzG:T base pair as well. More significantly, O^6-BzG was a stronger block than O^6-MeG to polymerization, causing polymerase stalling.

EXPERIMENTAL PROCEDURES

Enzymes. T7$^-$ and RT were expressed and purified in this laboratory as previously described (*23*) using stock plasmids provided by K. A. Johnson (T7$^-$ and thioredoxin, University of Texas, Austin, TX) (*24*, *25*) and S. Hughes (RT, Frederick Cancer Facility, Frederick, MD) (*26*). Protein concentrations for each experiment were determined using ϵ_{280} values of 144 mM^{-1} cm^{-1} for T7$^-$, 13.7 mM^{-1} cm^{-1} for thioredoxin, and 522 mM^{-1} cm^{-1} for RT (*27*). UV spectra were recorded using a Cary 14/OLIS spectrophotometer (On-Line Instrument Systems, Bogart, GA).

Nucleoside Triphosphates. Unlabeled Ultrapure Grade dNTPs were purchased from Amersham-Pharmacia Biotech (Piscataway, NJ). [γ-^{32}P]ATP was purchased from NEN Life Science (Boston, MA).

Oligonucleotides. All oligonucleotides, except the 36-mer oligonucleotide containing O^6-BzG, were purchased as "trityl-off" oligonucleotides from Midland Certified (Midland, Texas) or Operon Technologies (Alameda, CA). Gel electrophoresis purification was done using gels containing 8.0 M urea and 16% acrylamide (w/v) (from a 19:1 acrylamide:bisacrylamide solution, AccuGel, National Diagnostics, Atlanta, GA), which were run in 1× TBE buffer. Following separation, bands were excised and the oligonucleotides were eluted from crushed gel overnight in 500 mM $NH_4CH_3CO_2$ (pH 7.5) containing 1.0 mM EDTA. Following removal of acrylamide, oligonucleotides were desalted using Sephadex G-10 columns (Pharmacia, Piscataway, NJ). Purity was determined by CGE on a Beckman P/ACE 2000 instrument (Fullerton, CA) using a 27 cm × 100 μm eCAP capillary filled with Beckman 100-R ssDNA gel. Samples were applied at 10 kV for 10 s and separated at 11 kV (30 °C) in Tris-borate-urea buffer (from Beckman). The extinction coefficients for the oligonucleotides, determined by the Borer method (*28*), were as follows: 24-mer, ϵ_{260} = 224 mM^{-1} cm^{-1}; 25C-mer, ϵ_{260} = 230 mM^{-1} cm^{-1}; 25T-mer, ϵ_{260} = 232 mM^{-1} cm^{-1}; 26C-mer, ϵ_{260} = 240 mM^{-1} cm^{-1}; 26T-mer, ϵ_{260} = 243 mM^{-1} cm^{-1}; and 36-mer, ϵ_{260} = 310 mM^{-1} cm^{-1}.

Synthesis of O^6-Bz-dG Phosphoramidite and Site-Specifically Modified 36-mer. O^6-Bz-dG phosphoramidite was synthesized using Aldrich chemicals (Milwaukee, WI), unless otherwise indicated, according to a previously published procedure (*29*) with slight modification. N^2-Phenoxyacetyl-5′-*O*-(4,4′-dimethoxytrityl)-2′-deoxyguanosine, purchased from Sigma Chemicals (St. Louis, MO), was reacted with 1-(trimethylsilyl)imidazole in anhydrous conditions under argon. The reaction was monitored by analytical TLC [CH_2Cl_2:CH_3OH:$(C_2H_5)_3N$, 94.5:5:0.5, v/v/v] (R_f 0.4) using silica gel 60 F, visualized by UV light (254 nm). Next, a Mitsunobu reaction (*30*) was performed without purification of the first product. Triphenylphosphine, benzyl alcohol (1.6 molar equivalent), and diethyl azodicarboxylate were added successively to the reaction, which was heated at 95 °C for 15 min and slowly cooled overnight. Tetrabutylammonium fluoride (1.6 molar equivalent) was added to deprotect the deoxyribose 3′-hydroxyl group. The product was extracted and then isolated on preparative TLC plates (prewashed with acetone) using a 94.5:5:0.5 mixture of CH_2Cl_2/CH_3OH/$(C_2H_5)_3N$ (v/v/v). Extractions were done using a 99.5:0.5 (v/v) mixture of acetone/$(C_2H_5)_3N$ (2 × 50 mL) and CH_2Cl_2/CH_3OH/$(C_2H_5)_3N$ (94.5:5:0.5, 2 × 50 mL). The O6 substitution was confirmed by deprotecting a small portion of the 5′-DMT-N^2-PheAc-O^6-Bz-dG for analysis by HPLC (t_R 55 min). For isolation of O^6-Bz-dG, an octadecylsilane (C_{18}) 4.6 × 250 mm YMC-Pack ODS-AQ column, 5 μm, was used with a Spectra-Physics 8700 pumping system (Thermo-Separation Products, Piscataway, NJ). The solvent system used for purification was CH_3OH (solvent B) in 50 mM $NH_4CH_3CO_2$ (pH 4.5, solvent A) at a flow rate of 1.0 mL min^{-1} using the following gradient: 0 min (95% A, 5% B), 20 min (80% A, 20% B), 30 min (70% A, 30% B), 40 min (50% A, 50% B), 50 min (30% A, 70% B), 60 min (0% A, 100% B), and 70 min (95% A, 5% B). The O^6-substituted product was analyzed by UV spectroscopy: λ_{max} 287 nm (pH 2.0), λ_{max} 281 and 247 nm (pH 7.0), λ_{max} 280 and 247 nm (pH 12.0). The 5′-DMT-N^2-PheAc-O^6-Bz-dG was reacted with 2-cyanoethyl-*N*,*N*,*N*′,*N*′-tetraisopropylphosphorodiamidite and 1*H*-tetrazole, and the reaction was monitored by TLC (R_f 0.75). The reaction was quenched with 5% aq. $NaHCO_3$ (w/v), with extraction of the product using CH_2Cl_2 (3 × 5 mL); the organic layer was then dried over Na_2SO_4. Flash column chromatography (1.5 × 20 cm) was performed using silica gel 60 (70−230 mesh) to isolate the

product with a stepwise gradient of 99.5:0:0.5 to 97.5:2:0.5 of $CH_2Cl_2/CH_3OH/(C_2H_5)_3N$ (v/v/v). The product was dried in vacuo and concentrated in CH_3CN (PerSeptive Biosystems, Framingham, MA) for oligonucleotide synthesis. The 36-mer oligonucleotide was synthesized using an Expedite nucleic acid synthesis system (PerSeptive Biosystems) on a 1-μmol scale using benzoyl and isobutyryl protective groups. To compensate for phosphoramidite hydrolysis, the DNA adduct nucleoside solution (100 mg mL^{-1}) was made twice as concentrated as the standards. After overnight deprotection in 0.10 N NaOH, the beads from the cassette were pelleted, the solution was neutralized, and the beads were washed three times with water. The supernatant was lyophilized three times before gel purification, and purity was confirmed by CGE (see Supporting Information). To confirm the presence of O^6-BzG, the 36-mer (1.0 A_{260} unit = ~2.9 nmol) was digested into nucleosides in two steps using nuclease P1, snake venom phosphodiesterase (*Crotalus adamanteus* venom, Pharmacia), and alkaline phosphatase in a previously published procedure (*31*). The nucleosides were analyzed on a 4.6 × 250 mm YMC-Pack ODS-AQ HPLC column (5 μm) connected to a Hitachi L-7100 pumping system and were resolved with the above solvents at 1.0 mL min^{-1} using the following gradient: 0 min (100% A, 0% B), 10 min (80% A, 20% B), 20 min (50% A, 50% B), 40 min (20% A, 80% B), 55 min (0% A, 100% B), 65 min (0% A, 100% B), and 70 min (100% A, 0% B). Using this gradient, O^6-Bz-dG eluted at t_R 45.6 min. The presence of the O^6-BzG in the intact oligonucleotide was confirmed using MALDI/TOF MS (see Supporting Information).

Buffers and Reaction Conditions for Enzyme Assays. Unless indicated otherwise, all RT reactions were performed at 37 °C (*32*) in 50 mM Tris-HCl buffer (pH 7.5 at 37 °C) containing 50 mM NaCl. All T7$^-$ reactions were performed at 22 °C (*33*). For each experiment, T7$^-$ was reconstituted immediately prior to use. Thioredoxin was prepared separately in buffer containing 5 mM DTT without BSA, and T7$^-$ was prepared in buffer without DTT and BSA. T7$^-$ was then reconstituted so that T7$^-$ and thioredoxin were in a 1:20 molar ratio (*24*) with a final buffer composition of 40 mM Tris-HCl (pH 7.5 at 22 °C), 50 mM NaCl, 1.0 mM EDTA, 10 mM DTT, and 9.5 μg BSA mL^{-1}. All reactions were initiated by addition of dNTP so that the final buffer composition was 50 mM Tris-HCl (pH 7.4 at 22 °C) containing 12.5 mM $MgCl_2$.

Labeling/Annealing. The primer (200 pmol) was 5′-end-labeled using T4 polynucleotide kinase and purified on a Biospin column (BioRad, Hercules, CA). Template (36-mer) and ^{32}P-labeled primer (1.5:1 molar ratio) were annealed in 50 mM Tris-HCl buffer (pH 7.4) containing 2.0 mM β-mercaptoethanol and 5 mM $MgCl_2$ by heating at 90 °C for 10 s and slowly cooling to 22 °C overnight.

Steady-State Reactions. A ^{32}P-labeled primer, annealed to either an unmodified or adducted template, was extended in the presence of a single dNTP. The reaction was initiated by adding an equal volume of dNTP-Mg^{2+} to a preincubated E•DNA complex (100 nM DNA duplex) so that the ratio of primer/template to enzyme in the 8 μL reaction volume was at least 10:1. Enzyme concentrations and reaction times were chosen so that maximal product formation would be ~20% of the substrate concentration (*34*). For both T7$^-$ and RT, the unmodified primer/template was extended in the presence of 0.5 nM enzyme for 3 min. In the presence of either O^6-MeG or O^6-BzG (or when using the unmodified template with a dNTP other than dCTP), the reaction was done in the presence of 2−10 nM enzyme for 5 or 10 min. Each reaction was done at six dNTP concentrations (in triplicate) so that the final dNTP concentration was at least 5× the estimated K_m. After the appropriate time, reactions were quenched with 2 volumes (16 μL) of 20 mM EDTA (pH 9.4) in 95% formamide (w/v) and run on a denaturing polyacrylamide gel. The percentage of incorporation into the primer was quantitated using a model 400E PhosphorImager (Molecular Dynamics, Sunnyvale, CA) using Image Software, version 3.3. A graph of rate vs dNTP concentration was fit using nonlinear regression in GraphPad Prism Version 2.0b (San Diego, CA) for the determination of k_{cat} and K_m values.

Pre-Steady-State Reactions. Pre-steady-state kinetics were performed using a model RQF-3 KinTek chemical quench flow apparatus (KinTek Corp., Austin, TX) with 50 mM Tris-HCl (pH 7.4) buffer containing 5 mM $MgCl_2$ and 1.0 mM EDTA in the drive syringes. The reaction was initiated when the preequilibrated polymerase•DNA complex in sample syringe A (12.5 μL) was mixed with the dNTP-Mg^{2+} in syringe B (10.9 μL). The reactions were quenched with 0.3 M EDTA (pH 9.4) after reaction times of 5 ms to 5 s. Reactions were combined with 450 μL of formamide-dye solution and run on a denaturing gel, with analysis as described for the steady-state reactions. The burst rate was determined via single-exponential analysis from the negative slope of the line of $\ln(P_0 - P_t)$ vs t, where P_0 = product concentration at the end of the burst phase and P_t = product concentration at time, t. The points were fit in Prism to the burst equation $y = A(1 - e^{-k_p t}) + k_{ss}t$, where A = burst amplitude, k_p = pre-steady-state rate of nucleotide incorporation, t = time, and k_{ss} = steady-state rate of nucleotide incorporation (*24*, *35*). The % burst of incorporation was determined by dividing the burst amplitude of product by the concentration of enzyme. Enzyme concentration was determined from the UV absorbance of the enzyme stock (prepared in buffer) for a particular reaction. The enzyme and DNA concentration used in a particular pre-steady-state reaction are stated in the figure legends.

Determination of K_d^{dNTP}. K_d^{dNTP} values were determined by performing a succession of rapid quench reactions at six different dNTP concentrations with reaction times varying from 0.005 to 0.4 s. The burst rate (k_{obs}) from each of the six reactions was determined, and a graph of k_{obs} vs [dNTP] was plotted. This graph was fit to a hyperbola in Prism using the equation $k_{obs} = [k_{pol}[dNTP]/([dNTP] + K_d)]$, where k_{pol} = maximal rate of nucleotide incorporation and $K_d^{(dNTP)}$ = ground-state binding constant of dNTP (*24*, *35*).

RESULTS

The sequence of the 24-mer/36-mer duplex chosen for this study (Table 1) was successfully employed in previous polymerase studies with T7$^-$ and RT in this laboratory (*23*, *36*). In addition, the duplex region of this DNA primer/template (24 nucleotides) is long enough to accommodate the DNA binding sites of T7$^-$ and RT (*37*, *38*). T7$^-$ and RT were selected for use in this study for several reasons, including availability in large quantities and ease of purification (*24*, *26*), the need for only one (T7$^-$) or no (RT)

Table 1: Oligonucleotides Used in These Studies

24-mer	**5′** GCCTCGAGCCAGCCGCAGACGCAG
25C-mer	**5′** GCCTCGAGCCAGCCGCAGACGCAG**C**
25T-mer	**5′** GCCTCGAGCCAGCCGCAGACGCAG**T**
26C-mer	**5′** GCCTCGAGCCAGCCGCAGACGCAG**C**G
26T-mer	**5′** GCCTCGAGCCAGCCGCAGACGCAG**T**G
36-mer	**3′** CGGAGCTCGGTCGGCGTCTGCGTC**G***-CTCC-TGCGGCT[a]

[a] **G*** = unmodified G, *O*^{6}-MeG, or *O*^{6}-BzG.

Table 2: Steady-State Kinetic Parameters for One-Base Incorporation at Position 25[a]

enz	dNTP inserted	template	K_m (μM)	k_{cat} (s^{-1}) ($\times 10^{-3}$)	incorp efficiency (k_{cat}/K_m) ($\times 10^{-3}$)	f[a]
T7$^-$						
	C	G	1.7 ± 0.7	280 ± 30	160	
		O^6-MeG	75 ± 6	9.6 ± 0.3	0.13	
		O^6-BzG	530 ± 70	4.4 ± 0.3	0.0082	
	T	G	82 ± 10	1.6 ± 0.1	0.020	0.0001
		O^6-MeG	45 ± 7	40 ± 2	0.89	6.9
		O^6-BzG	89 ± 9	9.7 ± 0.4	0.11	13
RT						
	C	G	0.03 ± 0.01	120 ± 5	4000	
		O^6-MeG	19 ± 1	13 ± 3	0.68	
		O^6-BzG	93 ± 18	20 ± 1	0.22	
	T	G	230 ± 40	9.3 ± 0.6	0.040	<0.0001
		O^6-MeG	7.8 ± 0.9	9.9 ± 0.3	1.3	1.9
		O^6-BzG	190 ± 20	20 ± 1	0.11	0.5

[a] f (misinsertion frequency) $\cong (k_{cat}/K_m)$dNTP/$(k_{cat}/K_m)_{dCTP}$ where dNTP ≠ dCTP.

accessory proteins, and their extensive previous use as model replicative polymerases. Recent studies of mammalian polymerase δ in this laboratory (*39*, *40*) show that polymerase δ behaves much like T7$^-$ and RT in kinetic studies, validating use of T7$^-$ and RT as model polymerases to study the effect of guanyl O6 substituents on polymerase fidelity.

Steady-State Kinetics of dCTP and dTTP Incorporation Opposite G, O^6*-MeG, and* O^6*-BzG.* Steady-state parameters were measured for dNTP incorporation into 24-mer/36-mer duplexes opposite G, *O*^{6}-MeG, or *O*^{6}-BzG (Table 2). Steady-state reactions were performed using each of the four normal dNTPs, but incorporation of dATP and dGTP by T7$^-$ and RT opposite the adducts was much less inefficient than incorporation of dCTP and dTTP (results not shown). Thus, results shown focus on the kinetics of incorporation for dCTP, to form the "correct" base pair, and dTTP, to form the noncanonical base pair.

For incorporation of dCTP opposite G, *O*^{6}-MeG, and *O*^{6}-BzG, the K_m of T7$^-$ increased as a function of the bulk of the O6 substituent, while the inverse relationship was noted for k_{cat} (Table 2). The incorporation efficiency (k_{cat}/K_m) of T7$^-$ for dCTP insertion opposite G was 3 orders of magnitude greater as compared to dCTP incorporation opposite *O*^{6}-MeG. The high K_m for dCTP incorporation opposite *O*^{6}-BzG (530 ± 70 μM) caused additional reduction in the incorporation efficiency of T7$^-$ (by another order of magnitude) as compared to the efficiency of T7$^-$ at *O*^{6}-MeG. Steady-state parameters for incorporation of dTTP opposite *O*^{6}-MeG and *O*^{6}-BzG were also a function of the O6 substituent. Interestingly, the incorporation efficiency of dTTP incorporation opposite *O*^{6}-BzG was only 5-fold greater than for the formation of the G:T mispair. Misinsertion frequencies, defined as $f \cong (k_{cat}/K_m)_{dNTP}/(k_{cat}/K_m)_{dCTP}$ [where dNTP ≠ dCTP (*41*)], reflect the preference for the correct or incorrect nucleotide during incorporation. T7$^-$ incorporation of dTTP was greatly preferred over incorporation of the correct nucleotide, dCTP, for both *O*^{6}-MeG and *O*^{6}-BzG in steady-state conditions.

The ability of RT to incorporate dCTP opposite G, *O*^{6}-MeG, and *O*^{6}-BzG also depended upon the bulk at the O6 position of guanine (Table 2). The individual steady-state parameters k_{cat} or K_m did not follow a clear trend, but the efficiencies (k_{cat}/K_m) did. RT was more than 3 orders of magnitude more efficient at incorporating dCTP opposite G when compared to both *O*^{6}-MeG and *O*^{6}-BzG and was 3-fold more efficient at incorporating dCTP opposite *O*^{6}-MeG as compared to *O*^{6}-BzG. Interestingly, the incorporation efficiencies for dCTP and dTTP differed only 2-fold for both *O*^{6}-MeG and *O*^{6}-BzG. Thus, the misinsertion frequency for *O*^{6}-MeG was 1.9 (i.e., RT was somewhat more efficient at incorporating dTTP) and 0.5 for *O*^{6}-BzG (i.e., RT had a slight preference for dCTP incorporation).

Pre-Steady-State Kinetics of dCTP and dTTP Insertion Opposite G, O^6*-MeG, and* O^6*-BzG.* Steady-state analysis is useful for general polymerase characterization of nucleotide incorporation preferences, but steady-state kinetics are complicated by the overall slow step of DNA dissociation from the polymerase (*18*). Pre-steady-state kinetic analysis of dCTP and dTTP incorporation opposite *O*^{6}-MeG and *O*^{6}-BzG allows examination of a single reaction cycle (*17*, *24*). Pre-steady-state kinetic experiments, with the DNA concentration 3-fold greater than the enzyme concentration, were performed in a rapid-quench flow instrument. Preformed E•DNA complexes were mixed with saturating dNTP-Mg^{2+} (1−3 mM dNTP, except when using unmodified templates and correct dNTP, then 200 μM dNTP) and then quenched following mixing times between 0.005 and 5 s (Figure 1). The first phase of the cycle, i.e., the burst phase, was over by ~100 ms for both polymerases with the three different primer/template substrates, as determined by single-exponential analysis.

T7$^-$ incorporation of dCTP into the 24-mer/36-G-mer occurred with a burst rate of $k_p = 31 \pm 1\ s^{-1}$ (Table 3), as determined from the burst equation $y = A(1 - e^{-k_p t}) + k_{ss}t$. The burst rate of incorporation opposite *O*^{6}-MeG occurred at a 2-fold slower rate and a 4-fold slower rate opposite *O*^{6}-BzG. The percentage of T7$^-$ incorporation occurring in the burst phase, i.e., the burst amplitude, differed significantly when comparing the unmodified 24-mer/36-G-mer vs the duplexes containing *O*^{6}-MeG and *O*^{6}-BzG. The burst amplitude of product formation with the 24-mer/36-G-mer (dCTP incorporation) was 82% of the enzyme concentration, which is nearly stoichiometric (Figure 1A). In strong contrast, the burst amplitudes for *O*^{6}-MeG and *O*^{6}-BzG were 6 and 2%, respectively, indicating that only a small portion of the enzyme was competent in product formation. A similar trend was seen when T7$^-$ incorporated the wrong nucleotide (dTTP) into the adducted DNA. The burst rates only differed by 2-fold as compared to dCTP incorporation into the unmodified DNA (Table 3), but the burst amplitudes were again dramatically reduced, to 12% for *O*^{6}-MeG and 2% for *O*^{6}-BzG (Figure 1B).

RT incorporation differed somewhat from that of T7$^-$. Incorporation of dCTP across from G by RT occurred at $k_p = 26 \pm 3\ s^{-1}$, with the burst rates of *O*^{6}-MeG and *O*^{6}-BzG

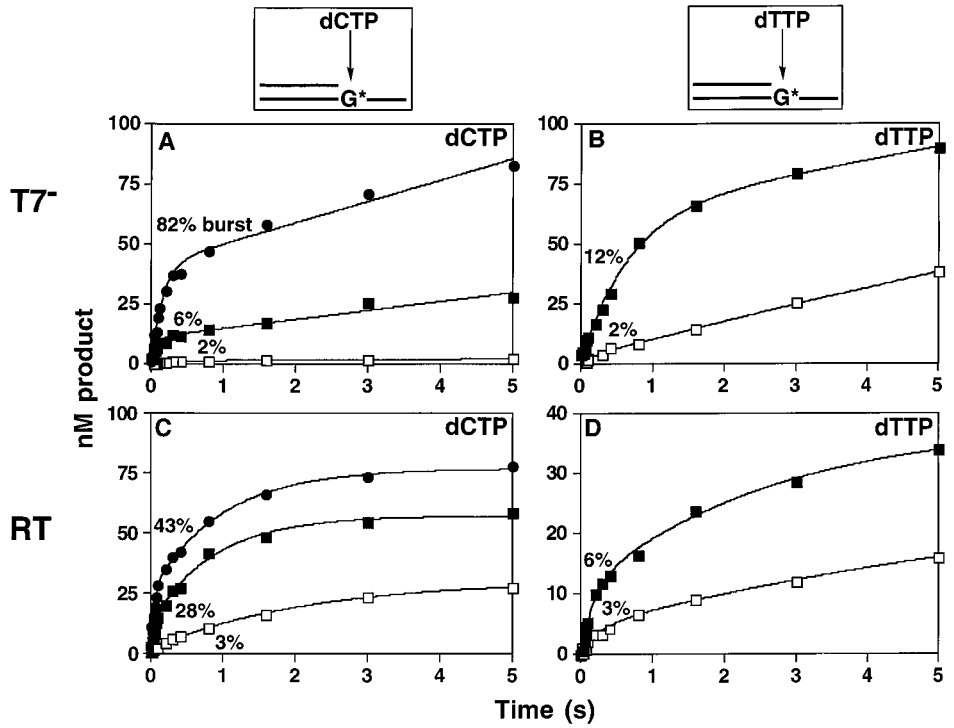

FIGURE 1: Pre-steady-state burst kinetics of incorporation across from G (●), O^6-MeG (■), or O^6-BzG (□). (A) T7$^-$ (23 nM) was incubated with 100 nM 24-mer/36-G-mer in the rapid quench-flow instrument and mixed with 200 μM dCTP to initiate the reaction. The pre-steady-state rate was determined from the burst equation, $y = A(1 - e^{-k_p t}) + k_{ss}t$, as described in the Experimental Procedures. The percentage of incorporation occurring in the burst phase for each reaction is indicated in the figure. T7$^-$ (170 nM), preincubated with 250 nM 24-mer/36-O^6-MeG-mer, was mixed with 2.0 mM dCTP to begin polymerization. T7$^-$ (65 nM) was incubated with 100 nM 24-mer/36-O^6-BzG-mer and mixed with 1.0 mM dCTP. (B) T7$^-$ (118 nM) was incubated with 250 nM 24-mer/36-O^6-MeG-mer or 180 nM T7$^-$ with 250 nM 24-mer/36-O^6-BzG-mer. The reaction was started with addition of 1.0 mM dTTP or 3.0 mM dTTP. (C) RT (69 nM) was incubated with 100 nM 24-mer/36-G-mer, 78 nM RT with 100 nM 24-mer/36-O^6-MeG-mer, or 80 nM RT with 100 nM 24-mer/36-O^6-BzG-mer, followed by mixing with 1.0 mM dCTP (200 μM dCTP for unmodified template) to initiate the reaction. (D) RT (140 nM) was incubated with 100 nM 24-mer/36-O^6-MeG-mer or 92 nM RT was incubated with 100 nM 24-mer/36-O^6-BzG-mer and mixed with 1.0 mM dTTP. All reactions were quenched with EDTA at the indicated times. Results for individual reactions are also displayed as separate plots in Figures 8 and 9 (as well as Figures 2 and 3) of the following paper in this issue (*21*).

Table 3: Pre-Steady-State Parameters for G, O^6-MeG, and O^6-BzG

		T7$^-$		RT		
primer/ template	dNTP inserted	k_p[a] (s^{-1})	% burst[b]	k_p (s^{-1})	% burst	k_{pol}[c] (s^{-1})
24/G	dCTP	31 ± 1	82	26 ± 3	43	25 ± 1
24/O^6-MeG	dCTP	16 ± 2	6	12 ± 2	28	26 ± 1
24/O^6-BzG	dCTP	7 ± 2	2	13 ± 2	3	23 ± 1
24/O^6-MeG	dTTP	13 ± 1	12	15 ± 1	6	28 ± 2
24/O^6-BzG	dTTP	11 ± 3	2	4 ± 2	3	20 ± 1
25C/G	dGTP	32 ± 1	100	31 ± 2	98	
25C/O^6-MeG	dGTP	23 ± 1	79	25 ± 1	41	
25C/O^6-BzG	dGTP	22 ± 1	35	17 ± 2	16	
25T/O^6-MeG	dGTP	27 ± 2	85	29 ± 1	82	
25T/O^6-BzG	dGTP	16 ± 1	13	26 ± 1	72	
26C/G	dATP	24 ± 2	80	23 ± 2	85	
26C/O^6-MeG	dATP	22 ± 1	100	23 ± 2	67	
26C/O^6-BzG	dATP	16 ± 1	25	17 ± 2	46	
26T/G	dATP	—[d]	—	18 ± 2	54	
26T/O^6-MeG	dATP	20 ± 5	100	26 ± 1	58	
26T/O^6-BzG	dATP	14 ± 1	66	22 ± 1	24	

[a] Pre-steady-state burst rate. [b] Percentage of enzyme that turns over product in burst phase. [c] Maximum rate of dNTP incorporation. [d] No burst phase.

differing by 2-fold (Table 3). A 43% burst was observed for incorporation of dCTP into the unmodified 24-mer/36-G-mer (Figure 1C), which is not uncommon for RT because it often binds unmodified DNA and RNA substrates in a nonproductive manner (*42*). Incorporation of dCTP into a 24-mer/36-O^6-MeG-mer occurred with a modest burst of 28%, which differs from T7$^-$ kinetics, whereas incorporation of dCTP across from O^6-BzG by RT gave only a 3% burst (Figure 1C). Very small burst amplitudes were observed for both adducts during incorporation of dTTP by RT, 6% for O^6-MeG and 3% for O^6-BzG (Figure 1D), similar to those observed during T7$^-$ polymerization.

Table 4: Steady-State Kinetic Parameters of Next-Base Extension (Insertion of dGTP)

enzyme	template: **primer**	K_m^{dGTP} (μM)	k_{cat} (s^{-1}) ($\times 10^{-3}$)	extension efficiency (k_{cat}/K_m) ($\times 10^{-3}$)
T7$^-$				
	G:**C**	0.20 ± 0.04	900 ± 70	4600
	O^6-MeG:**C**	1.0 ± 0.1	100 ± 4	100
	O^6-BzG:**C**	0.30 ± 0.04	60 ± 1	220
	G:**T**	630 ± 90	180 ± 10	0.3
	O^6-MeG:**T**	1.7 ± 0.2	210 ± 7	130
	O^6-BzG:**T**	50 ± 8	120 ± 6	2
RT				
	G:**C**	0.02 ± 0.004	560 ± 20	34000
	O^6-MeG:**C**	3 ± 0.5	75 ± 3	22
	O^6-BzG:**C**	50 ± 6	140 ± 4	3
	G:**T**	130 ± 30	70 ± 3	0.6
	O^6-MeG:**T**	0.4 ± 0.1	140 ± 4	320
	O^6-BzG:**T**	1.1 ± 0.2	88 ± 4	77

Steady-State and Pre-Steady-State Kinetics of Next-Base Extension Following dCTP or dTTP Insertion. Steady-state kinetic analysis of next-base extension (Table 4) was done to establish if the preference of each enzyme is to extend the correct base pair, G*:C, or the mispair, G*:T, in the presence of the next correct nucleotide for this sequence, dGTP (Table 1). These reactions were performed by anneal-

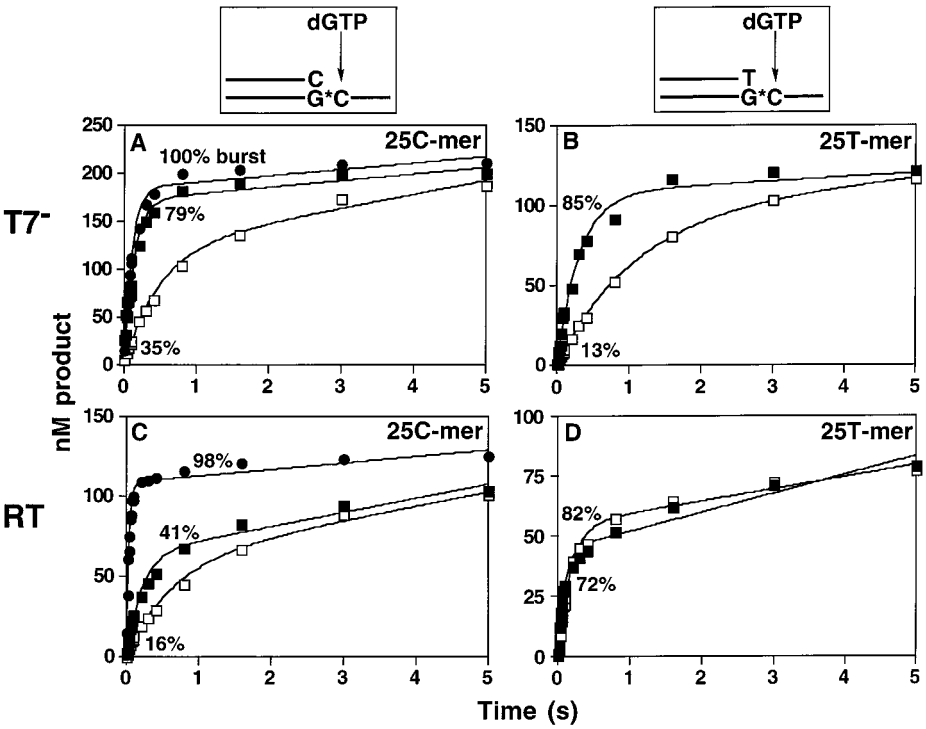

FIGURE 2: Pre-steady-state burst kinetics of next-base extension of the "correct" base pair (G*:C) or the noncanonical base pair (G*:T). Templates were annealed to a 25C-mer or a 25T-mer, indicating 25-mer primers terminating (3′) in C (dCTP incorporation) or T (dTTP incorporation), respectively. Either G (●), O^6-MeG (■), or O^6-BzG (□) was at position 25 on the DNA template (see Table 1); insertion of dGTP occurred at position 26. (A) T7$^-$ (72 nM) was incubated with 200 nM 25C-mer/36-G-mer in the rapid quench-flow instrument. Reaction at each time point was initiated by addition of 200 μM dGTP. The burst rate was determined from the burst equation, $y = A(1 - e^{-k_p t}) + k_{ss}t$, as described in the Experimental Procedures. The percentage of incorporation occurring in the burst phase for each reaction is indicated in the figure. T7$^-$ (106 nM) was incubated with 250 nM 25C-mer/36-O^6-MeG-mer or 74 nM T7$^-$ was incubated with 250 nM 25C-mer/36-O^6-BzG-mer and mixed with 2.0 mM dGTP to initiate the reaction. (B) T7$^-$ (39 nM) was incubated with 150 nM 25T-mer/36-O^6-MeG-mer or 75 nM T7$^-$ was incubated with 150 nM 25T-mer/36-O^6-BzG-mer. Each reaction was initiated with the addition of 2.0 mM dGTP. (C) RT (85 nM) was incubated with 150 nM 25C-mer/36-G-mer. Reactions were initiated by addition of 200 μM dGTP. RT (64 nM) was incubated with 150 nM 25C-mer/36-O^6-MeG-mer or 73 nM RT was incubated with 150 nM 25C-mer/36-O^6-BzG-mer and mixed with 2.0 mM dGTP. (D) A preincubated solution of RT (35 nM) with 100 nM 25T-mer/36-O^6-MeG-mer or 34 nM RT with 100 nM 25T-mer/36-O^6-BzG-mer was mixed with 1.0 mM dGTP, thus initiating the reaction. All reactions were quenched with EDTA at the indicated times.

ing a 25-mer, which had either a C or a T at the 3′ end, to one of the three 36-mer templates. T7$^-$ and RT extended the canonical base pair G:C much more easily than any of the adduct-containing base pairs, as reflected by the 2 or 3 order of magnitude differences in extension efficiencies for G:C vs the other base pairs. T7$^-$ extended the O^6-MeG:C and O^6-MeG:T pairs with similar efficiency but greatly preferred to extend the "correct" base pair O^6-BzG:C in preference to O^6-BzG:T. RT behaved differently than T7$^-$ in that it extended both of the base pairs O^6-MeG:T and O^6-BzG:T much more efficiently than O^6-MeG or O^6-BzG paired with C.

The pre-steady-state kinetic results (Figure 2) agreed with the general trend established by the steady-state kinetics. T7$^-$ extended the G:C base pair (incorporation into the 25C-mer/36-G-mer) with a $k_p = 32 \pm 1$ s^{-1} (Table 3) and ~100% stoichiometric burst amplitude (Figure 2A). Burst rates for T7$^-$ with the O^6-alkylG base pairs were all similar to that of the G:C base pair, except for the extension of the O^6-BzG:T pair (incorporation into the 25T-mer/36-G-mer) where the burst rate was half that for the G:C base pair (Table 3). The burst amplitudes for extension of the O^6-MeG:C and O^6-MeG:T base pairs by T7$^-$ were similar in magnitude, 79 and 85%, respectively, reflecting the results of the steady-state assays. Extension of the 25C-mer/36-O^6-BzG-mer yielded a larger burst amplitude than extension of the 25T-mer/36-O^6-BzG-mer, the duplex containing the G*:T mispair, 35% as compared to 13% (Figure 2A,B).

RT also extended the normal G:C base pair with a stoichiometric burst. Most of the burst rates obtained for the O^6-alkylG-containing duplexes were similar to those obtained for the unmodified duplex ($k_p = 31 \pm 2$ s^{-1}), except for the 25C-mer/36-O^6-BzG-mer, which had a 2-fold lower rate (Table 3). RT had difficulty extending both O^6-MeG:C and O^6-BzG:C base pairs, yielding burst amplitudes of only 41 and 16% (Figure 2C). On the other hand, the enzyme had little difficulty extending the O^6-MeG:T and O^6-BzG:T base pairs, i.e., nearly stoichiometric bursts (Figure 2D). With the exception of the extension of O^6-MeG:C by RT, neither polymerase encountered appreciable difficulty during extension of an O^6-MeG-containing duplex as compared to incorporation opposite O^6-MeG. Thus, extension of duplexes containing the bulkier O^6-BzG was much more difficult for both enzymes as compared to those containing O^6-MeG, except for RT extension of the O^6-BzG:T base pair.

Pre-Steady-State Kinetics of Incorporation Two Bases Beyond O^6*-AlkylG.* Pre-steady-state kinetic analysis was performed using 26-mer primers with either a C (26C-mer) or a T (26T-mer) at position 25 (across from G*) to access the effect of O^6-alkylG on incorporation two bases past the

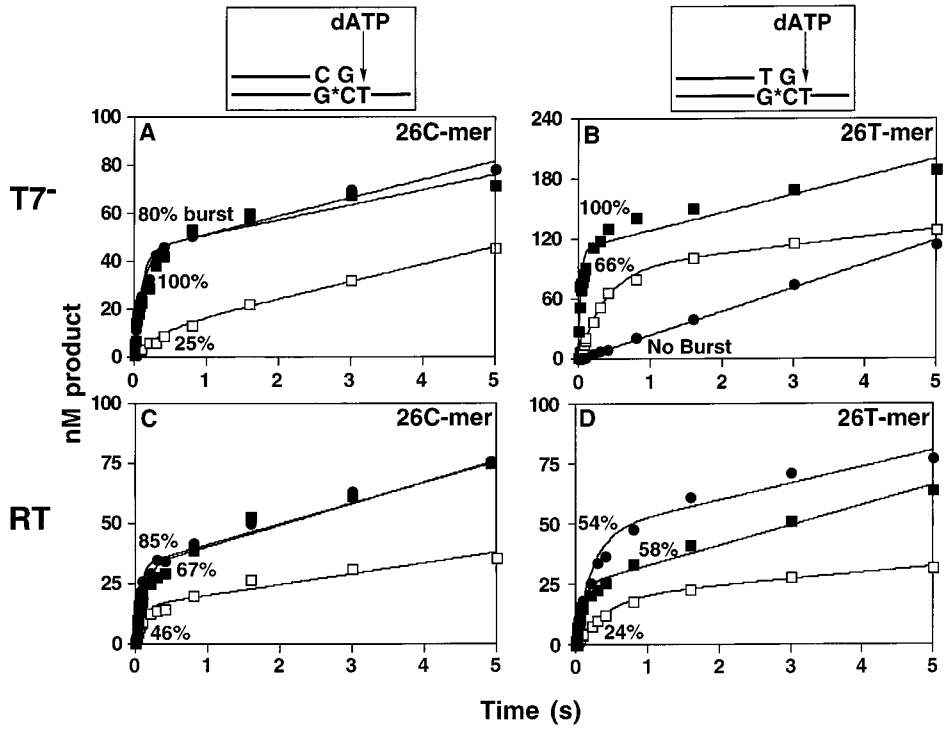

FIGURE 3: Pre-steady-state burst kinetics of incorporation two bases beyond O^6-alkylG. Insertion of dATP occurred at position 27 with either G (●), O^6-MeG (■), or O^6-BzG (□) at position 25 on the DNA template. Either a C (26C-mer) or a T (26T-mer) was inserted at position 25 of the primer, which is across from G or O^6-alkylG in the template (see Table 1). (A) T7$^-$ (33 nM) was incubated with 100 nM 26C-mer/36-G-mer in the rapid quench-flow instrument. Reactions were initiated by the addition of 200 μM dATP. The burst rate was determined from the burst equation, $y = A(1 - e^{-k_p t}) + k_{ss}t$, as described in the Experimental Procedures. The percentage of incorporation occurring in the burst phase for each reaction is indicated in the figure. T7$^-$ (22 nM), incubated with 100 nM 26C-mer/36-O^6-MeG-mer, was mixed with 200 μM dATP to initiate the reaction. T7$^-$ (28 nM) was incubated with 100 nM 26C-mer/36-O^6-BzG-mer and mixed with 1.0 mM dATP. (B) T7$^-$ (114 nM) was incubated with 250 nM 26T-mer/36-G-mer. Reaction was initiated by addition of 1.0 mM dATP, and data were fit to a straight line. T7$^-$ (46 nM), incubated with 200 nM 26T-mer/36-O^6-MeG-mer, was mixed with 1.0 mM dATP. T7$^-$ (33 nM) was incubated with 150 nM 26T-mer/36-O^6-BzG-mer and mixed with 1.0 mM dATP to initiate the reaction. (C) RT (31 nM) was incubated with 100 nM 26C-mer/36-G-mer. Reaction was initiated by addition of 200 μM dATP. RT (29 nM) was incubated with 100 nM 26C-mer/36-O^6-MeG-mer, or RT (34 nM) was incubated with 100 nM 26C-mer/36-O^6-BzG-mer. Each reaction was mixed with 1.0 mM dATP to initiate the reaction. (D) RT (35 nM) was combined with 100 nM 26T-mer/36-G-mer, 31 nM RT with 100 nM 26T-mer/36-O^6-MeG-mer, or 38 nM RT with 100 nM 26T-mer/36-O^6-BzG-mer, followed by mixing with 1.0 mM dATP. All reactions were quenched with EDTA at the indicated times.

lesion (Figure 3). Incorporation of dATP at position 27 by T7$^-$ (i.e., two bases after the target G) showed stoichiometric bursts for both O^6-MeG:C and O^6-MeG:T (Figure 3A,B), indicating that the O^6-MeG adduct no longer exhibits a significant effect on polymerization. In addition, the rate of incorporation with both O^6-MeG-containing duplexes was very close to that of the unmodified duplex (Table 3). Interestingly, the O^6-BzG:C base pair was preferentially extended by T7$^-$, but at two bases beyond the adduct (incorporation into 26C-mer/36-O^6-BzG-mer), a low burst amplitude (25%) was observed at position 27 on the oligonucleotide. Incorporation into the 26T-mer/36-O^6-BzG-mer resulted in a burst amplitude of 66%, despite the fact that the O^6-BzG:T base pair was not a favorable substrate during next-base extension (Figure 3B). Although incorporation opposite O^6-BzG greatly hindered T7$^-$ polymerization, polymerization two bases beyond O^6-BzG was not significantly affected. This result contrasts with the incorporation two bases beyond the G:T mispair, which demonstrated no burst (linear kinetics) indicating that the chemistry of bond formation had become rate-limiting overall (Figure 3B).

During RT-catalyzed polymerization, the burst amplitude of both O^6-MeG:C and O^6-BzG:C increased two bases beyond the adduct site to 67 and 41%, respectively (Figure 3C), as compared to results seen for next-base extension. Rates were very close to that of the unmodified duplex [k_p = 23 s^{-1} (O^6-MeG) and k_p = 17 s^{-1} (O^6-BzG) vs k_p = 23 s^{-1} (Table 3)]. RT was able to incorporate dATP at position 27 on a duplex that contained a G:T mispair at position 25 with a surprisingly high burst amplitude of 54%. Interestingly, incorporation into the 26T-mer/36-O^6-MeG-mer and the 26T-mer/36-O^6-BzG-mer duplexes showed burst amplitudes of 58 and 24%, respectively (Figure 3D). These percentages are lower than the burst amplitudes seen for next-base extension, i.e., incorporation at position 26; however, these lower burst amplitudes correlate with gel electrophoresis polymerization assays done in the presence of all four dNTPs (*21*), which show an accumulation of product at position 26.

Determination of K_d^{dCTP} and K_d^{dTTP} for dNTP Incorporation by RT. Analysis of the change in the pre-steady-state burst rate as a function of increasing dNTP concentration yields K_d^{dNTP}, a measure of the binding affinity of the dNTP to the E•DNA complex to form a complex poised for catalysis. K_d^{dNTP} reflects the formation of the productive ternary complex because initial dNTP binding is followed by a rate-limiting conformational change to the productive complex, which is then converted into product (*24*). The burst rate from each reaction was determined. Then, the resulting

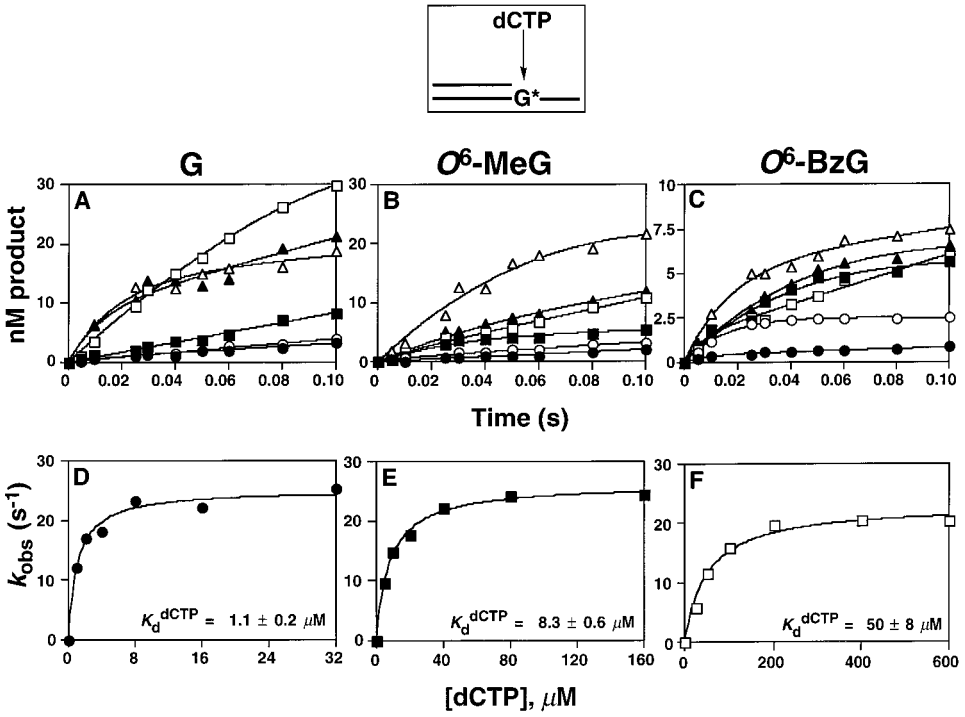

FIGURE 4: Determination of K_d^{dCTP} by analysis of dCTP concentration dependence of the pre-steady-state burst rate. All reactions were quenched with EDTA over the range 0.005 to 0.4 s. Time points in the burst phase (up to 100 ms) are displayed to illustrate the changes in the slopes of the lines. (A) RT (60−80 nM) was incubated with 100 nM 24-mer/36-G-mer and mixed with increasing dCTP concentrations: 1 μM, ●; 2 μM, ■; 4 μM, ○; 8 μM, □; 16 μM, ▲; 32 μM, △. (B) RT (120−140 nM), preincubated with 200 nM 24-mer/36-O^6-MeG-mer, was mixed with increasing dCTP concentrations: 5 μM, ●; 10 μM, ○; 20 μM, ■; 40 μM, □; 80 μM, ▲; 160 μM, △. (C) RT (130−155 nM) was incubated with 200 nM 24-mer/36-O^6-BzG-mer; E•DNA was then mixed with increasing dCTP concentrations: 25 μM, ●; 50 μM, ○; 100 μM, ■; 200 μM, □; 400 μM, ▲; 600 μM, △. (D) After determining the burst rates (k_{obs}) from each of the six reactions in panel A, a graph of k_{obs} vs [dCTP] was plotted and fit to a hyperbola (Prism software) using the equation $k_{obs} = [k_{pol}[dCTP]/([dCTP] + K_d)]$, where k_{pol} = maximal rate of nucleotide incorporation and K_d = ground-state binding constant of dCTP. (E) Burst rates (k_{obs}) from each of the six reactions in panel B were plotted vs [dCTP] to determine k_{pol} and K_d^{dCTP}. (F) The burst rate (k_{obs}) of each of the six reactions in panel C was determined; a graph of k_{obs} vs [dCTP] yielded k_{pol} and K_d^{dCTP}.

k_{obs} values were plotted as a function of [dNTP] and fit to a hyperbola using the equation $k_{obs} = [k_{pol}[dNTP]/([dNTP] + K_d)]$, where k_{pol} is the maximal rate of nucleotide incorporation and K_d^{dNTP} is the ground-state binding constant for dNTP. The K_d^{dNTP} values for incorporation of the correct (Figure 4) and incorrect dNTPs (Figure 5) for the three 24-mer/36-mer duplexes were determined for RT but not for T7$^-$.[2]

The K_d^{dCTP} for incorporation into the 24-mer/36-G-mer by RT was 1.1 ± 0.2 μM (Figure 4D). The tight binding of dCTP to the unmodified DNA duplex reflects the ability of RT to easily form the productive ternary complex. The k_{pol} for RT with the 24-mer/36-G-mer and dCTP was 25 ± 1 s^{-1} (Table 3). The K_d^{dCTP} for the O^6-MeG-containing DNA duplex increased 8-fold over the unmodified DNA duplex to 8.3 ± 0.6 μM (Figure 4E), reflecting the instability caused by the DNA modification. A 50-fold increase in the K_d^{dCTP} (50 ± 8 μM) was observed when RT replicated the O^6-BzG-containing substrate (Figure 4F). Interestingly, the maximum rate of incorporation with the modified templates did not change much for the adducted templates when compared to the unmodified template [k_{pol} = 26 ± 1 s^{-1} for O^6-MeG; k_{pol} = 23 ± 1 s^{-1} for O^6-BzG (Table 3)].

The K_d^{dTTP} for the 24-mer/36-O^6-MeG-mer was 8.6 ± 2.2 μM (Figure 5C), which is not significantly different from the binding constant for the correct nucleotide. The K_d^{dTTP} for the O^6-BzG-containing DNA duplex, 77 ± 17 μM (Figure 5D), was significantly higher than for the O^6-MeG substrate. In addition, the K_d^{dTTP} for O^6-BzG was somewhat higher than the K_d^{dNTP} determined for formation of the ternary complex with the correct dNTP. Again, although the K_d^{dNTP} varied as a function of the O6 substituent, the maximum rates of incorporation did not vary considerably from the unmodified DNA duplex [k_{pol} = 28 ± 2 s^{-1} for O^6-MeG and k_{pol} = 20 ± 1 s^{-1} for O^6-BzG (Table 3)].

DISCUSSION

Polymerase kinetics can provide valuable insight into how genomic integrity is maintained by discerning the details of the enzymology of DNA replication. Surprisingly, the application of polymerase enzymology to understanding fidelity is a relatively new field. Kornberg and his associates discovered the first polymerase, DNA polymerase I of *E. coli*, in 1956 (*43*, *44*), but 30 years elapsed before detailed investigations of the mechanism of nucleotide incorporation began (*17*). In the early 1990s, the minimal mechanism of polymerization was fully elucidated (*24*), and this mechanistic knowledge has subsequently been applied to under-

[2] The pre-steady-state studies of T7$^-$ with O^6-alkylG-containing oligonucleotides (Figure 1A,B) presented more technical difficulties than the studies with RT. The experiments with T7$^-$ required high levels of enzyme and DNA in the presence of saturating dNTP concentrations to determine the pre-steady-state burst rate. Thus, detection of incorporation with subsaturating dNTP concentrations caused an unacceptable level of error due to the low rates.

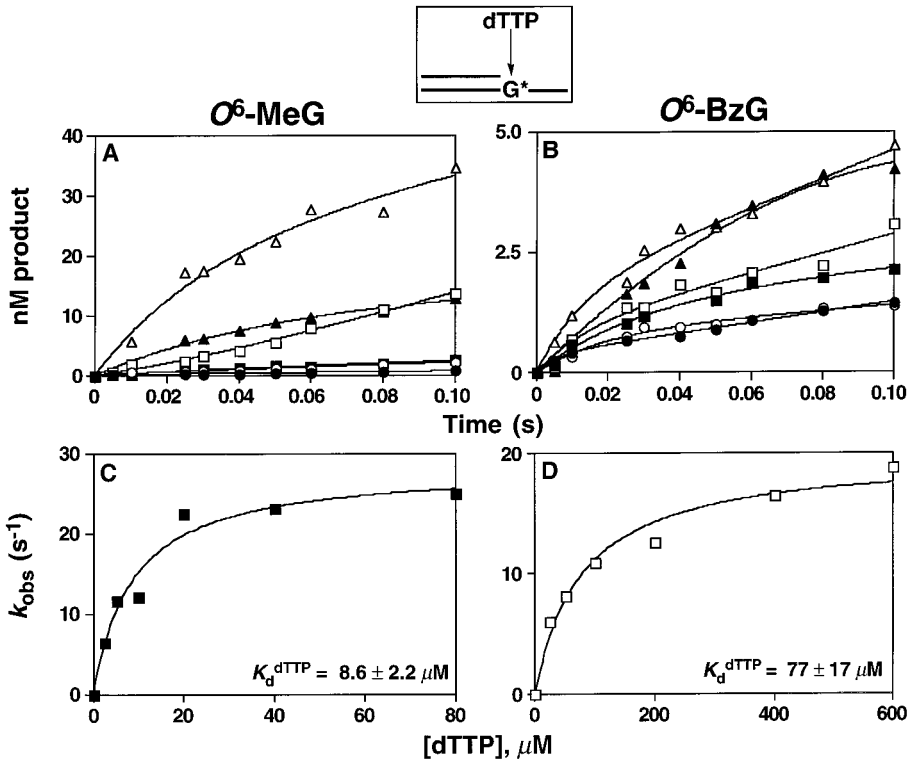

FIGURE 5: Determination of K_d^{dTTP} by examining dTTP concentration dependence of the pre-steady-state burst rate for O^6-alkylG-containing templates. All reactions were quenched with EDTA over the range 0.005 to 0.4 s. Time points in the burst phase (up to 100 ms) are displayed to illustrate the changes in the slopes of the lines. (A) RT (125−145 nM) was incubated with 200 nM 24-mer/36-O^6-MeG-mer, and the reaction was started by mixing with increasing amounts of dTTP: 2.5 μM, ●; 5 μM, ○; 10 μM, ■; 20 μM, □; 40 μM, ▲; 80 μM, △. (B) RT (130−150 nM) was incubated with 200 nM 24-mer/36-O^6-BzG-mer, followed by subsequent mixing with increasing concentrations of dTTP: 25 μM, ●; 50 μM, ○; 100 μM, ■; 200 μM, □; 400 μM, ▲; 600 μM, △. (C) The burst rate (k_{obs}) from each of the six reactions in panel A was determined, and a graph of k_{obs} vs [dTTP] was plotted. This graph was fit to a hyperbola (Prism software) using the equation $k_{obs} = [k_{pol}[dTTP]/([dTTP] + K_d)]$, where k_{pol} = maximal rate of nucleotide incorporation and K_d = ground-state binding constant of dTTP. (D) After determining the burst rates (k_{obs}) from each of the six reactions in panel B, a graph of k_{obs} vs [dTTP] was plotted to determine the k_{pol} and K_d^{dTTP}.

standing how polymerases maintained genomic integrity in the presence of DNA modifications, including DNA−carcinogen adducts. Pre-steady-state kinetics were used in this study to address the question of how T7$^-$ and RT (which function as true replication enzymes) maintain fidelity during replication of DNA containing the highly mutagenic O^6-MeG or the bulkier O^6-BzG, which has been reported to be less miscoding but more likely to cause polymerase stalling (*22*).

Both steady-state and pre-steady-state kinetics of nucleotide incorporation were performed in this study. Pre-steady-state kinetic analysis (done with DNA in excess of enzyme) reveals two phases of incorporation. The first phase, or burst phase, is a rapid accumulation of product in the first enzyme turnover, due to a rate-limiting conformational change before phosphodiester bond formation during incorporation involving the normal bases (*18*, *24*). The amplitude of this burst phase corresponds to the amount of enzyme that rapidly converts substrate to product; during incorporation of the four canonical bases, the burst amplitude usually approximates the enzyme concentration. A nonstoichiometric burst (where product concentration is less than the amount of enzyme present) indicates that not all of the enzyme can form product rapidly. The second phase, or the steady-state phase, is governed by the rate-limiting step in multiple turnovers of normal incorporation, probably DNA dissociation (*45*).

Surprisingly, the pre-steady-state rates of incorporation (k_p) opposite O^6-alkylG were no more than 6-fold different than for incorporation opposite G (Table 3). Also, there was no significant difference in the rates of incorporation of dCTP or dTTP opposite O^6-alkylG. The presence of an O6 substituent reduced the pre-steady-state burst rate for T7$^-$ by 2-fold for incorporation of either dCTP or dTTP opposite O^6-MeG and by 3- to 4-fold for dTTP or dCTP incorporation opposite O^6-BzG, respectively. When compared to incorporation opposite G, the presence of an O^6-alkylG reduced the burst rate for RT by 2-fold except when dTTP was incorporated opposite O^6-BzG, where a 6-fold difference was measured. This pattern contrasts with the KF results obtained by Tan et al. (*20*), in which the pre-steady-state rate of incorporation of dTTP opposite O^6-MeG was 5-fold less than for dCTP incorporation (with even greater assumed differences as compared to unmodified DNA).

Tan et al. (*20*) did not observe biphasic kinetics for the incorporation of dCTP opposite O^6-MeG by KF; thus, either the conformational change or phosphodiester bond formation presumably became the rate-limiting step. In our own work with T7$^-$ and RT, turnover of each E•DNA•dNTP complex containing O^6-MeG or O^6-BzG clearly demonstrated biphasic kinetics (Figures 1−3). Although the burst rates (k_p) measured with O^6-alkylG-containing DNA did not differ much from those with unmodified DNA (Table 3), the burst amplitudes were greatly reduced. Only a 2 to 3% burst

amplitude was observed for O^6-alkylG-containing DNA, except for T7$^-$ incorporation of dTTP opposite O^6-MeG (12%) and RT incorporation of dCTP opposite O^6-BzG (28%) (Figure 1). Tan et al. (*20*) did not discuss the reduced burst amplitude observed for dTTP incorporation opposite O^6-MeG, but a comparison of the amount of product formed during the burst and the enzyme concentration in the reaction indicates that the burst is not stoichiometric. Unfortunately, comparisons between the repair enzyme KF and the replicative enzymes T7$^-$ and RT are difficult to interpret because differences between polymerases can result in varying effects of a DNA adduct on replication.

Adducts affect DNA structure and, subsequently, polymerase fidelity and kinetics to varying extents. Even small changes, such as addition of a methyl to the O6 position of G, can have significant effects on fidelity. Misincorporation percentages [defined as misincorporation % = $f/(1 + f)$, where $f \cong (k_{cat}/K_m)_{dTTP}/(k_{cat}/K_m)_{dCTP}$] (*41*) predict that T7$^-$ greatly prefers to insert dTTP rather than dCTP opposite both O^6-MeG and O^6-BzG (87% for O^6-MeG and 93% for O^6-BzG) (Table 3). RT showed only slight preference for dTTP incorporation opposite O^6-MeG (65%) and demonstrated a slight preference for dCTP incorporation opposite O^6-BzG (67%), which contrasts with the strong tendencies displayed by T7$^-$. In a previous study of T7$^-$ and RT with 8-oxoG, another adduct with a small change in its chemical structure (*23*), an opposite trend was noted: T7$^-$ exhibited a moderate preference for incorporation of dCTP (63%), but RT had a very strong preference for dATP incorporation (93%). These steady-state results reveal only general enzyme preferences for dNTPs (*45*), whereas pre-steady-state kinetics can give information about the chemistry of phosphodiester bond formation as well as the conformational change preceding bond formation.

Previous pre-steady-state studies with T7$^-$ and RT and 8-oxoG (*23*) only demonstrated biphasic kinetics when T7$^-$ incorporated the correct base dCTP opposite 8-oxoG and RT incorporated dATP opposite 8-oxoG. Incorporation of dATP opposite 8-oxoG by RT was the first reported example of biphasic kinetics observed for incorporation of the "wrong" base pair partner opposite 8-oxoG. In contrast, biphasic kinetics were observed for incorporation of either dCTP or dTTP opposite both O^6-MeG and O^6-BzG (Figure 1). The burst amplitudes observed during incorporation opposite 8-oxoG (*23*) were much higher than those observed for O^6-alkylG adducts (2−28%), indicating that O^6-alkylG is more of a hindrance to polymerization than 8-oxoG.

While incorporation opposite an adduct provides some information about polymerase fidelity, it also important to determine if the G*:C base pair or the noncanonical G*:T base pair is preferentially extended (G* = modified G). RT preferred to extend both the O^6-MeG:T and O^6-BzG:T base pairs (as compared to O^6-MeG:C and O^6-BzG:C), indicated by the large burst amplitudes (Figure 2). Thus, formation of product by RT occurred readily during the burst phase. Similarly, many polymerases prefer to extend the noncanonical base pair, e.g., Furge and Guengerich (*23*) where 8-oxoG:A was a much better substrate for T7$^-$ and RT extension than 8-oxoG:C. In our present work, T7$^-$ preferentially extended the "correct" base pair O^6-BzG:C but displayed very similar kinetics for extension of O^6-MeG:C and O^6-MeG:T (burst amplitudes of 79 and 85%, respectively) (Figure 2A,B). Although T7$^-$ extended both O^6-MeG base pairs equally, dTTP was preferentially inserted over dCTP opposite O^6-MeG, consistent with the high mutagenic potential of O^6-MeG in vivo (*22*).

Although the addition of a methyl at the O6 position represents a small change in the size of guanine, it does change the tautomeric structure of G. Therefore, base pairs containing O^6-MeG do cause some distortions in the DNA helix (*14*) and probably in the transition state prior to incorporation of a dNTP opposite O^6-MeG. Although no structural work has examined how O^6-BzG affects the DNA duplex, it has a more dramatic effect on polymerase kinetics than O^6-MeG, and thus it may affect DNA structure more than its less bulky counterpart. Another adduct that causes major DNA distortions, i.e., a large kink of 39−55°, is an intrastrand cross-link of cisplatin (*46*). Studies of the interaction of cisplatin−DNA with T7$^-$ and RT by Suo et al. (*47*) indicate that both enzymes show a large reduction in the burst amplitude at the site of both cross-linked guanines. RT was affected an additional base after the site of adduction, and T7$^-$ polymerization was affected five bases after the cisplatin adduct. Suo et al. (*47*) rationalized the results by hypothesizing that T7$^-$ is more sensitive to the changes in DNA caused by cisplatin because T7$^-$ does not have as much flexibility in its active site as RT, which accepts both DNA and RNA substrates. The O^6-alkylG adducts affected T7$^-$ and RT differently. O^6-MeG did not affect T7$^-$ polymerization two bases after the site of the adduct, but RT demonstrated altered kinetics from normal incorporation at this position, i.e., lower burst amplitudes (Figure 3). O^6-BzG affected both polymerases two bases beyond the adduct site, but neither T7$^-$ nor RT was affected at position 28, i.e., three bases beyond the adduct (results not shown). Thus, although O^6-alkylG adducts affect polymerization of T7$^-$ and RT one or two bases downstream from the actual site of modification, other adducts (e.g., cisplatin-G) disrupt nucleotide incorporation to a greater extent.

Suo et al. (*47*) reported that cisplatin affected the ground-state binding of nucleotides, i.e., altered K_d^{dNTP}, at sites of incorporation downstream from the adduct. The determination of a large K_d^{dNTP} suggests that the productive E•DNA•dNTP complex may not readily form in the presence of a DNA−carcinogen adduct. Thus, changes in the enzyme, DNA, or both must occur for bond formation to occur. The K_d^{dNTP} for T7$^-$ was 85 (± 18) μM for incorporation one base beyond the cisplatin adduct, similar to the K_d^{dNTP} determined at the site of the adduct for RT with O^6-BzG (50 ± 8 μM for dCTP and 77 ± 17 μM for dTTP) (Figures 4F and 5D). This result indicates that cisplatin−DNA is more disruptive to polymerization than O^6-BzG since the K_d^{dNTP} downstream of cisplatin-G is greater than the K_d^{dNTP} at the O^6-BzG site.

T7$^-$ and RT exhibited differences in incorporation kinetics with O^6-MeG and O^6-BzG as well as differences in nucleotide preference. These results demonstrate that adducts with similar basic structures, i.e., substitution at the O6 position of G, can have different effects on a polymerase. Lindsley and Fuchs (*48*) demonstrated that incorporation opposite AF-G and its more distorting acetylated derivative, AAF-G, also have different effects on T7$^-$ (*48*). Choice of nucleotide

for insertion opposite the two adducts differed, and AF-G caused less stalling of T7$^-$ than did AAF-G. Incorporation opposite AAF-G demonstrated monophasic kinetics, which differs significantly from our results obtained with O^6-alkylG. Although incorporation opposite both O^6-MeG and O^6-BzG demonstrated biphasic kinetics, O^6-BzG gave much smaller burst amplitudes and larger downstream effects (Figures 1−3). Thus, although O^6-BzG and AAF-G both stalled T7$^-$, the adducts affected the polymerase differently. For O^6-BzG the burst amplitude is reduced; during incorporation opposite AAF-G the conformational change or chemistry of bond formation apparently becomes rate-limiting in the steady-state (i.e., monophasic kinetics).

Polymerization can be greatly affected by the presence of a DNA adduct or any other structural change in the DNA, such as a DNA hairpin (*49*), but simple mispairs of the canonical A, C, G, and T bases are even more disruptive to polymerization. Wong et al. (*50*) studied the effects of A:A, A:C, and A:G mispairs on polymerization by T7$^-$. Monophasic kinetics were observed during formation of all of these mispairs, indicating that the rate-limiting step was no longer DNA dissociation but the rate of conformational change or phosphodiester bond formation. In our study, a 26T-mer/36-G-mer (containing a G:T mispair at position 25) was used as a control substrate to look at polymerization two bases beyond the adduct (Figure 3). Surprisingly, RT did not have any difficulty incorporating at position 27 on a 26T-mer/36-G-mer substrate, probably due to its more flexible active site. The 26T-mer/36-G-mer greatly affected T7$^-$ kinetics as in the case of the substrates of Wong et al. (*50*), and monophasic kinetics (no burst) were observed even two bases after the G:T mispair. In contrast, incorporation opposite or beyond O^6-MeG and O^6-BzG by T7$^-$ demonstrated biphasic kinetics (Figures 1−3). Although the burst amplitudes were small (indicating that the E•DNA•dNTP complex was not efficiently being turned over into product), a step following bond formation was still the overall rate-limiting steady-state step for polymerization of oligonucleotide containing an O^6-alkylG, unlike kinetics observed with mispairs (*50*).

Kinetic analysis allows elucidation of polymerase enzymology in a simplified system, but the information must also be considered in the context of in vivo mutagenesis, which requires the concerted action of several polymerases (*51*). Moschel and his associates have found that O^6-BzG is two or three times less mutagenic than O^6-MeG in both *E. coli* and mammalian cells (*22*, *52*, *53*). This difference in mutagenicity is due to two factors—more efficient repair of O^6-BzG by alkyltransferases (*54*) and an apparently lower miscoding potential of O^6-BzG. In addition, O^6-MeG and O^6-BzG display different mutational spectra at some DNA sequences. O^6-BzG can cause different kinds of mutations, including G → T and G → C mutations in addition to the expected G → A mutation, but O^6-MeG only causes G → A mutations (*22*).

Can mutagenesis results be reconciled by kinetic analysis of replication of O^6-MeG and O^6-BzG by model polymerases T7$^-$ and RT? Interestingly, steady-state analysis demonstrated that both dATP and dGTP could be incorporated opposite O^6-BzG by T7$^-$ much more efficiently than O^6-MeG (results not shown),[3] which may explain why varied mutations are seen in the presence of O^6-BzG. Although steady-state kinetics indicated a preference for dTTP over dCTP, pre-steady-state kinetic analysis for insertion of dCTP or dTTP opposite O^6-BzG was very similar for both T7$^-$ and RT (Figure 1). In addition, the preference for a primer/template containing an O^6-BzG:C base pair or O^6-BzG:T base pair differed between T7$^-$ and RT and also depended on whether incorporation occurred at position 26 or 27 (Figures 2 and 3). Thus, pre-steady-state kinetic analysis indicates that neither dCTP nor dTTP is preferentially inserted opposite O^6-BzG, and neither of the resulting primer/templates can be extended easily. These results may explain why the bulkier O^6-BzG is less miscoding than its smaller counterpart because both polymerases preferred to extend the O^6-MeG:T base pair in pre-steady-state analysis.

Although the pre-steady-state kinetics of these model polymerases correlated with in vivo mutagenesis results, this analysis is oversimplified because neither T7$^-$ nor RT is the polymerase involved in the bacterial or mammalian cell mutagenicity experiments. In addition, the recent discovery of specialized polymerases complicates the understanding of in vivo mutagenesis as it is not clear which polymerase replicates when certain DNA adducts are present (*55*). Our pre-steady-state analysis did show, however, that the bulkier structure of O^6-BzG caused the polymerase to stall at and beyond the site of the adduct more than O^6-MeG. This stalling of the polymerases by O^6-BzG is significant as it may signal for the action of specialized polymerases.

Pre-steady-state kinetics of model polymerases can be valuable in understanding how adducts affect polymerization and can be applicable to mammalian systems. Other studies in this laboratory (*39*, *40*) have shown that polymerase δ, the major leading-strand mammalian polymerase, behaves very similarly to the polymerases studied here. Since polymerase δ utilizes the same steps of the minimal mechanism of incorporation as the model replicative polymerases, some general knowledge of how O^6-alkylG perturbs fidelity can be gained from this study.

In summary, pre-steady-state analysis indicated that when polymerization does occur on an O^6-BzG-containing substrate, no strong preference is seen for dCTP or dTTP insertion and neither O^6-BzG:C nor O^6-BzG:T is preferentially extended, unlike the case of the less bulky O^6-MeG. Thus, the fidelity of T7$^-$ and RT, much like those polymerases involved in bacterial and mammalian mutagenicity, is compromised more by O^6-MeG than the bulkier O^6-BzG. Importantly, O^6-BzG caused much polymerase stalling as T7$^-$ and RT had more difficulty inserting a nucleotide opposite O^6-BzG than O^6-MeG, as denoted by the lower pre-steady-state burst amplitudes (Figure 1). These lower burst amplitudes indicate that fewer E•DNA•dNTP complexes are being converted to product. In conclusion, pre-steady-state analysis indicated that although O^6-MeG is more miscoding, O^6-BzG is a greater block to polymerization by T7$^-$ and RT. The roles of individual reaction steps in misincorporation and stalling by T7$^-$ and RT are considered further in the following paper in this issue (*21*).

[3] The misinsertion frequency [defined as $f \cong (k_{cat}/K_m)_{dNTP}/(k_{cat}/K_m)_{dCTP}$ where dNTP ≠ dCTP (*41*)] of T7$^-$ for dATP incorporation opposite O^6-BzG was 3.8. The misinsertion frequency was 0.3 for dGTP incorporation opposite O^6-BzG. These values were 10- to 100-fold higher than the corresponding misinsertion frequencies of T7$^-$ for incorporation of dATP and dGTP opposite O^6-MeG.

ACKNOWLEDGMENT

We thank M.-S. Kim, L. Nechev, C. M. Harris, P. Tamura, H. Shimamura, and J. B. Wheeler for help in synthesis and characterization of the O^6-Bz-dG-containing 36-mer. We also thank S. Langouët, L. L. Furge, and H. J. Einolf for assistance in protein purification and kinetic analysis.

SUPPORTING INFORMATION AVAILABLE

Three figures give the characterization of the O^6-BzG-36-mer. Identity of the O^6-Bz-dG was confirmed by the HPLC analysis of the enzymatic digest of the oligonucleotide into nucleosides. The presence of the O^6-BzG adduct in the intact 36-mer was confirmed by MALDI/TOF MS. Purity of the O^6-BzG-36-mer was checked by CGE. This information is available free of charge via the Internet at http://pubs.acs.org.

REFERENCES

1. Marnett, L. J., and Burcham, P. C. (1993) *Chem. Res. Toxicol. 6*, 771−785.
2. Miller, J. A. , and Miller, E. C. (1971) *J. Natl. Cancer Inst. 47*, 5−14.
3. Guengerich, F. P. (1996) in *Control Mechanisms of Carcinogenesis* (Hengstler, J. G., and Oesch, F., Eds.) pp 12−35, Institut für Toxikologie, Mainz, Germany.
4. Dipple, A. (1995) *Carcinogenesis 16*, 437−441.
5. Echols, H., and Goodman, M. F. (1991) *Annu. Rev. Biochem. 60*, 477−511.
6. Singer, B., and Essigmann, J. M. (1991) *Carcinogenesis 12*, 949−955.
7. Shibutani, S., Takeshita, M., and Grollman, A. P. (1991) *Nature 349*, 431−434.
8. Singer, B., Chavez, F., Goodman, M. F., Essigmann, J. M., and Dosanjh, M. K. (1989) *Proc. Natl. Acad. Sci. U.S.A. 86*, 8271−8274.
9. Eisenbrand, G., Hofer, M., and Janzowski, C. (1996) in *Control Mechanisms of Carcinogenesis* (Hengstler, J. G., and Oesch, F., Eds.) pp 160−192, Institut für Toxikologie, Mainz, Germany.
10. Taverna, P., and Sedgwick, B. (1996) *J. Bacteriol. 178*, 5105−5111.
11. Loveless, A. (1969) *Nature 223*, 206−207.
12. Patel, D. J., Shapiro, L., Kozlowski, S. A., Gaffney, B. L., and Jones, R. A. (1986) *Biochemistry 25*, 1027−1036.
13. Patel, D. J., Shapiro, L., Kozlowski, S. A., Gaffney, B. L., and Jones, R. A. (1986) *Biochemistry 25*, 1036−1042.
14. Swann, P. F. (1990) *Mutat. Res. 233*, 81−94.
15. Voigt, J. M., and Topal, M. D. (1995) *Carcinogenesis 16*, 1775−1782.
16. Haracska, L., Prakash, S., and Prakash, L. (2000) *Mol. Cell. Biol. 20*, 8001−8007.
17. Mizrahi, V., Henrie, R. N., Marlier, J. F., Johnson, K. A., and Benkovic, S. J. (1985) *Biochemistry 24*, 4010−4018.
18. Kuchta, R. D., Mizrahi, V., Benkovic, P. A., Johnson, K. A., and Benkovic, S. J. (1987) *Biochemistry 26*, 8410−8417.
19. Johnson, K. A. (1993) *Annu. Rev. Biochem. 62*, 685−713.
20. Tan, H. B., Swann, P. F., and Chance, E. M. (1994) *Biochemistry 33*, 5335−5346.
21. Woodside, A. M., and Guengerich, F. P. (2002) *Biochemistry 41*, 1039−1050.
22. Mitra, G., Pauly, G. T., Kumar, R., Pei, G. K., Hughes, S. H., Moschel, R. C., and Barbacid, M. (1989) *Proc. Natl. Acad. Sci. U.S.A. 86*, 8650−8654.
23. Furge, L. L., and Guengerich, F. P. (1997) *Biochemistry 36*, 6475−6487.
24. Patel, S. S., Wong, I., and Johnson, K. A. (1991) *Biochemistry 30*, 511−525.
25. Lunn, C. A., Kathju, S., Wallace, B. J., Kushner, S. R., and Pigiet, V. (1984) *J. Biol. Chem. 259*, 10469−10474.
26. Le Grice, S. F. J., Cameron, C. E., and Benkovic, S. J. (1995) *Methods Enzymol. 262*, 130−144.
27. Furge, L. L., and Guengerich, F. P. (1999) *Biochemistry 38*, 4818−4825.
28. Borer, P. N. (1975) in *Handbook of Biochemistry and Molecular Biology, 3rd ed* (Fasman, G. D., Ed.) pp 589−590, CRC Press, Cleveland, OH.
29. Kim, M.-S., and Guengerich, F. P. (1997) *Chem. Res. Toxicol. 10*, 1133−1143.
30. Mitsunobu, O. (1981) *Synthesis* 1−28.
31. Langouët, S., Mican, A. N., Müller, M., Fink, S. P., Marnett, L. J., Muhle, S. A., and Guengerich, F. P. (1998) *Biochemistry 37*, 5184−5193.
32. Kati, W. M., Johnson, K. A., Jerva, L. F., and Anderson, K. S. (1992) *J. Biol. Chem. 267*, 25988−25997.
33. Huber, H. E., Tabor, S., and Richardson, C. C. (1987) *J. Biol. Chem. 262*, 16224−16232.
34. Goodman, M. F., Creighton, S., Bloom, L. B., and Petruska, J. (1993) *Crit. Rev. Biochem. Mol. Biol. 28*, 83−126.
35. Johnson, K. A. (1995) *Methods Enzymol. 249*, 38−61.
36. Einolf, H. J., Schnetz-Boutaud, N., and Guengerich, F. P. (1998) *Biochemistry 37*, 13300−13312.
37. Jacobo-Molina, A., Ding, J., Nanni, R. G., Clark, A. D., Jr., Lu, X., Tantillo, C., Williams, R. L., Kamer, G., Ferris, A. L., Clark, P., Hizi, A., Hughes, S. H., and Arnold, E. (1993) *Proc. Natl. Acad. Sci. U.S.A. 90*, 6320−6324.
38. Zinnen, S., Hsieh, J. C., and Modrich, P. (1994) *J. Biol. Chem. 269*, 24195−24202.
39. Einolf, H. J., and Guengerich, F. P. (2000) *J. Biol. Chem. 275*, 16316−16322.
40. Einolf, H. J., and Guengerich, F. P. (2001) *J. Biol. Chem. 276*, 3764−3771.
41. Boosalis, M. S., Petruska, J., and Goodman, M. F. (1987) *J. Biol. Chem. 262*, 14689−14696.
42. Wöhrl, B. M., Krebs, R., Goody, R. S., and Restle, T. (1999) *J. Mol. Biol. 292*, 333−344.
43. Kornberg, A., Lehman, I. R., Bessman, M. J., and Simms, E. S. (1956) *Biochim. Biophys. Acta 21*, 197−198.
44. Lehman, I. R., Bessman, M. J., Simms, E. S., and Kornberg, A. (1958) *J. Biol. Chem. 233*, 163−170.
45. Johnson, K. A. (1992) in *The Enzymes* (Boyer, P. D., Ed.) pp 1−61, Academic Press, Inc., New York.
46. Takahara, P. M., Rosenzweig, A. C., Frederick, C. A., and Lippard, S. J. (1995) *Nature 377*, 649−652.
47. Suo, Z., Lippard, S. J., and Johnson, K. A. (1999) *Biochemistry 38*, 715−726.
48. Lindsley, J. E., and Fuchs, R. P. P. (1994) *Biochemistry 33*, 764−772.
49. Suo, Z., and Johnson, K. A. (1998) *J. Biol. Chem. 273*, 27259−27267.
50. Wong, I., Patel, S. S., and Johnson, K. A. (1991) *Biochemistry 30*, 526−537.
51. Friedberg, E. C., and Gerlach, V. L. (1999) *Cell 98*, 413−416.
52. Pauly, G. T., Hughes, S. H., and Moschel, R. C. (1995) *Biochemistry 34*, 8924−8930.
53. Pauly, G. T., Hughes, S. H., and Moschel, R. C. (1994) *Biochemistry 33*, 9169−9177.
54. Goodtzova, K., Kanugula, S., Edara, S., Pauly, G. T., Moschel, R. C., and Pegg, A. E. (1997) *J. Biol. Chem. 272*, 8332−8339.
55. Goodman, M. F., and Tippin, B. (2000) *Nat. Rev. Mol. Cell Biol. 1*, 101−109.

BI011495N